Redox Biology 58 (2022) 102556

Contents lists available at ScienceDirect

Redox Biology

journal homepage: www.elsevier.com/locate/redox

Myristoyl lysophosphatidylcholine is a biomarker and potential therapeutic target for community-acquired pneumonia

Wengang Nan [a,1], Fen Xiong [b,1], Hong Zheng [b], Chen Li [b], Cong Lou [b], Xiong Lei [a], Huizhen Wu [a], Hongchang Gao [b,**], Yuping Li [a,*]

[a] Department of Respiratory and Critical Care Medicine, The First Affiliated Hospital of Wenzhou Medical University, Wenzhou, China
[b] Oujiang Laboratory (Zhejiang Lab for Regenerative Medicine, Vision and Brain Health), School of Pharmaceutical Sciences, Wenzhou Medical University, Wenzhou, China

ARTICLE INFO

Keywords:
Community-acquired pneumonia
Acute lung injury
Biomarker
Metabolomics
NLRP3 inflammasome

ABSTRACT

There is no gold standard for evaluating the severity of community-acquired pneumonia (CAP), and it is still based on a score. This study aimed to use the metabolomics method to find promised biomarkers in assessing disease severity and potential therapeutic targets for CAP. The result found that the metabolites in the plasma samples of CAP patients had significantly different between the acute phase and the remission phase, especially lysophosphatidylcholine (LPCs) in glycerophospholipids, whose levels are negatively linked to the severity of the disease. Subsequently, the two key metabolites of myristoyl lysophosphatidylcholine (LPC 14:0) and LPC 16:1 were screened. We analyzed the predictive performance of the two metabolites using Spearman-related analysis and ROC curves, and LPC14:0 showed more satisfactory diagnostic performance than LPC16:1. Then we explored the protective role and mechanism of LPC 14:0 in animal and cell models. The results showed that LPC 14:0 could inhibit the LPS-induced secretion of IL-1β, IL-6, and TNF-α, lower the ROS and MDA levels, and decreased the depletion of SOD and GSH, thereby reducing lung tissue and cell damage, such as down-regulating the protein level in BALF, lung W/D ratio, MPO activity, and apoptosis. We found that LPC 14:0 inhibited LPS-induced inflammatory response and oxidative stress, and the above protection was achieved by inhibiting LPS-induced activation of the NLRP3 inflammasome. LPC 14:0 may serve as a novel biomarker for predicting the severity of CAP. In addition, our exploration of the role of LPC 14:0 in animal and cellular models has reinforced its promise as a therapeutic target to improve the clinical efficacy for CAP.

1. Introduction

Community-acquired pneumonia (CAP) remains one of the most common causes of death worldwide, with a global incidence of CAP in adults ranging from 0.3% to 0.5% [1]. Owing to the abuse of drugs and the emergence of drug-resistant bacteria, the diagnosis and treatment of CAP still face severe challenges [2]. Failure to provide timely or correct diagnosis and treatment may lead to exacerbation and progression to severe CAP [3,4]. Mortality among outpatient CAP patients is less than 5%, compared with 5–10% and 35–40% among hospitalized and Intensive Care Unit (ICU) CAP patients, respectively [5,6]. Therefore, timely diagnosis and treatment can improve the prognosis of patients with CAP.

Metabolomics is a technique for the systematic analysis of small molecule metabolites in biological systems [7,8]. Some previous metabolomic studies on pneumonia have provided a powerful approach to finding new biomarkers for CAP [9–11]. For example, by analyzing the serum of CAP patients and non-CAP controls, Kelvin [10] has identified lipid metabolites as prospective diagnostic biomarkers by studying the sera of CAP and non-CAP patients. Ning P [11] found that sphingosine and dehydroepiandrosterone sulfate (DHEA-S) in serum are biomarkers that can distinguish non-severe CAP from severe CAP by a metabolomic method based on LC-MS/MS. However, the previous articles mainly focused on the discovery of CAP biomarkers, and there were

* Corresponding author. Department of Respiratory and Critical Care Medicine, The First Affiliated Hospital of Wenzhou Medical University, Nanbaixiang Street, Wenzhou, 325000, China.
** Corresponding author. Institute of Metabonomics & Medical NMR, School of Pharmaceutical Sciences, Wenzhou Medical University, Wenzhou, China.
E-mail addresses: gaohc27@wmu.edu.cn (H. Gao), wzliyp@163.com (Y. Li).
[1] These writers made the same contribution to this work.

https://doi.org/10.1016/j.redox.2022.102556
Received 29 October 2022; Received in revised form 18 November 2022; Accepted 24 November 2022
Available online 26 November 2022

few studies on the therapeutic targets and mechanisms of action related to biomarkers.

We performed metabolomic studies using ultra-performance liquid chromatography-tandem mass spectrometry (UHPLC-MS/MS) on plasma samples from CAP patients in the acute and remission phases to identify the metabolic characteristics at two periods. Differential metabolites were simultaneously screened to find biomarkers for evaluating disease severity and having prospects to be therapeutic targets. Lipopolysaccharide (LPS) is a common endotoxin, which plays an important role in the inflammatory reaction in the body. Previous studies have shown that the LPS concentration in sepsis patients is significantly higher than that in normal people [12]. To investigate the role of the identified metabolites in CAP, we validated them on a mouse acute lung injury (ALI) model and a RAW 264.7 cell inflammation model established by LPS [13,14]. Inflammation and oxidative stress are considered to be closely related events in CAP pathological processes [15,16]. Reactive oxygen species (ROS) are an important factor connecting oxidative stress to inflammation, and LPS can contribute to the generation of ROS, which activates the separation of the thioredoxin-interacting protein (TXNIP) from thioredoxin (TRX) and then combines with a nucleotide-binding domain-like receptor protein 3 (NLRP3), causing the activation of the NLRP3 inflammasome [17,18]. NLRP3 inflammasome, including an adaptor protein ASC, cysteine aspartate-specific protease-1 (Caspase-1), and NLRP3, has a significant impact on the body's immune defense and disease occurrence. The activation of the inflammasome will release a large number of mature inflammatory factors IL-1β and further stimulates the generation of the IL-6, and TNF-α [19–21]. Following up on the result, we explored the protective effects of myristoyl lysophosphatidylcholine (LPC 14:0) on LPS-induced ALI mice and inflammatory cells and their mechanisms related to inflammation and oxidative stress.

2. Materials and methods

2.1. Study population and design

Study participants were recruited from patients with CAP hospitalized in the Department of Respiratory Medicine or the Respiratory Intensive Care Unit (RICU) of the First Affiliated Hospital of Wenzhou Medical University, Wenzhou, China, from May 2020 to February 2021. This study was approved by the Ethics Committee of the First Affiliated Hospital of Wenzhou Medical University (No. 2020–111) and followed the Declaration of Helsinki (as revised in 2013). Every participant signed a written informed consent form.

In total, 163 participants were enrolled in the study, including 48 non-severe CAP patients, and 34 severe CAP patients, as well as an additional 81 healthy volunteers matched for gender and age as controls. The diagnosis of CAP was based on the 2016 CAP guidelines in China [22]. Exclusion criteria: Diagnosed with cancer or suffering from acute or chronic inflammatory diseases (such as nosocomial infection, active tuberculosis, rheumatoid arthritis, severe immunosuppression, etc.).

2.2. Sample acquisition and processing

Plasma samples were acquired from CAP at two-time points: the first day of admission (acute phase) and before discharge (remission phase). An appropriate amount of peripheral venous blood was drawn and injected into a tube containing heparin sodium, and let stand for half an hour at room temperature, then the supernatant was gathered after centrifugation at 3000*g* for 10 min.

400 μL of cold methanol: acetonitrile (v:v = 1:1) mixture was added to 200 μL of plasma samples to precipitate proteins, vortexed with 60 s, and the supernatant was collected by centrifugation. Then the supernatant was aliquoted into clean tubes, dried under N2 flow, and subsequently, redissolved in 100 μl ACN/water (1:1, v:v) for UHPLC-MS/MS analysis. The quality control (QC) sample solution contains equivalent amounts of plasma from each sample, with one QC sample randomly selected among 10 experimental samples.

2.3. Untargeted and targeted UHPLC-MS/MS analysis

Sample analysis was performed on a SHIMADZU CBM-30A Lite LC system (Shimadzu Corporation, Kyoto, Japan) using a Waters Acquity HSS T3 column (2.1 × 100 mm, 1.8 μm), which is compatible with API 6600 Triple TOF (AB SCIEX, Foster City, CA, USA) quality detector coupling. The specific experimental methods and data processing was based on the experimental protocol of Xiong F [23] and optimized for our particular situation, and the detailed protocol can be found in the supplementary methods.

After sample runs, raw data were collected by MassHunter workstation software and processed into mzXML format, followed by data pre-processing using XC-MS software (XC-MS plus, California, USA), including nonlinear retention time alignment, peak identification, filtering, alignment, matching, and identification.

2.4. Data analysis and metabolite identification

All data by LC-MS were normalized to sum and Pareto scale before single or multivariate data analysis. Multivariate analysis, including principal component analysis (PCA) and supervised orthogonal partial least squares discriminant analysis (OPLS-DA), was conducted with SIMCA 14.1 software (Umea Umetrics, Sweden). PCA can display the distribution characteristics of the dataset, while the OPLS-DA model can distinguish categories and show the differences between group samples more clearly, and generate corresponding variable importance projection (VIP) values. Models were validated by permutation test (n = 200) to avoid overfitting. R^2Y and Q^2 values can evaluate model performance, where R^2Y indicates the fit of the model and Q^2 indicates its predictability, and the more the values of these two parameters converge to 1.0, the more reliable the model is.

Univariate statistical analysis was performed through the online website Kido (https://www.omicshare.com/tools/) with a Student t-test.

Only variables that met the false discovery rate (FDR) values < 0.05, VIP values > 1.0 and fold change (FC) < 0.5 or FC > 2 were identified as significantly differential metabolites.

After screening for significantly different metabolites, these metabolites were further identified based on precise *m/z* values and MS/MS signature fragments and validated through HMDB 4.0. Heatmaps were drawn through the online site Metaboanalyst 5.0 (https://www.metaboanalyst.ca/). Venn diagrams were drawn through the online website (http://www.ehbio.com/).

2.5. Targeted UHPLC-MS/MS

A targeted assay was used to quantify LPC 14:0 and LPC 16:1 in human and mouse blood samples. Analyses were completed on a SHIMADZU CBM-30A Lite LC system together with an API 6500 Q-TRAP (AB SCIEX, Foster City, CA, USA) mass detector operated in ESI + mode. A Kinetex C18 100A column (100 × 2.1 mm, 2.6 μm) was utilized for lipids separation. The detailed protocol can be found in the supplementary methods.

LPC 14:0 (Sigma-Aldrich, >98% purity) standard solutions with concentrations ranging from 1 to 1000 ng/mL were prepared and concentration calibration curves were established. In addition, LPC 16:1 were measured by multiple reaction monitoring (MRM) using 1-Hexadecanoyl-2-lysophosphatidylcholine (LPC 16:0) (GlpBio, USA) as internal standard (200 ng/mL) and the methods were linear over concentrations of 1–1000 ng/mL. Metabolite concentrations were measured using AB SciexMultiQuant software (version 2.1, AB SCIEX, CA, USA).

2.6. Cell culture and CCK-8

RAW 264.7 cells (Chinese Cell Bank in Beijing, China) were cultured in DMEM medium containing 10% FBS, 100 U/mL penicillin, 100 U/mL streptomycins, and 3 mM glutamine at 37 °C with 5% carbon dioxide.

The effect in different drug concentrations of LPS (dissolved in Phosphate Buffered Saline (PBS)) and LPC14:0 (dissolved in 1% BSA, BSA diluted with PBS) for cell vitality was determined by CCK-8. The cells were inoculated in 96-well panels (1×10^4 cells/well) for 24 h and then replaced with serum-free medium to starve for 1 h. Firstly, cells were added to LPS (0.1, 1, 10, 20, 30) μg/mL for 12 h to find the appropriate model of cellular inflammation. Then, cells were cultured in two 96-well panels and pretreated with LPC 14:0 (10, 20, 30, 40) μM for 1 h, and one of the plates was exposed to LPS (1 μg/mL) for 12 h. Add 10ul CCK-8, incubate for 2h, and then measure the absorbance at 450 nm.

2.7. Quantification of apoptosis, measurement of ROS and antioxidant enzymes (GSH, SOD)

RAW 264.7 cells were cultured for 24 h, starved for 1 h, pretreated with LPC 14:0 (20 μM) for 1 h, and then exposed to LPS (20 μg/mL) for 12 h. The cells were collected by centrifugation for 5 min at 300 g after the administration. 1×10^5 cells were added with 5 μL FITC Annexin V and 5 μL propidium iodide (PI), incubated at 25 °C for 15 min protected from light. The percentages of apoptosis and necrosis were detected by flow cytometry.

To measure ROS, cells were collected and incubated with 1 mL of serum-free medium containing 1 μL of DCFH-DA at 37 °C for 20 min in the dark. After three washes with cold PBS, the DCF fluorescence intensity of cells was measured.

Furthermore, the cells were collected after the same treatment, disrupted by a sonicator, and the cell supernatant was used to assess the SOD and GSH levels using an assay kit.

2.8. Animals and experimental protocols

8-week-old SPF-grade male C57BL/6 mice were purchased from Zhejiang Weitong Lihua Laboratory Animal Technology Co., Ltd. (SYXK (Zhejiang) 2021–0017), and were reared adaptively for 1 week. All animals were raised under SPF conditions. All experiments involving animals were performed following the ethical policies and procedures approved by the Ethics Committee of Wenzhou Medical University, China (No.2021–0095).

For the first set of animals, Mice were divided into two subgroups, the control group (PBS +1% BSA) and the LPS group (5 mg/kg, dissolved in PBS). LPS was instilled into the trachea to induce ALI in mice.

The second set of mice were randomly divided into four subgroups: control group (PBS +1% BSA), LPC 14:0 only group (10 mg/kg dissolved in 1% BSA, BSA diluted with PBS) [24,25], LPS only group (5 mg/kg, dissolved in PBS), LPS (5 mg/kg) + LPC 14:0 (10 mg/kg) group. Mice were pretreated by subcutaneous injection of LPC 14:0 (10 mg/kg), anesthetized with isoflurane (5% induction, 2% maintenance) after 2 h, and LPS (5 mg/kg, diluted to 50ul with PBS) was instilled into the trachea to induce ALI in mice. LPC 14:0 (10 mg/kg) was subcutaneously administered once again 10 h after LPS administration in the trachea, and the control group was subcutaneously injected with 1% BSA and intratracheal instillation of PBS. Following LPS injection for 24 h, mice were anesthetized with isoflurane and executed by decortication, then mouse lung tissue specimens, bronchoalveolar lavage fluid (BALF), and serum were gathered and stored at −80 °C.

2.9. Lung hematoxylin-eosin (H & E) and the determination of BALF

Histopathological examination was performed on lung tissues from mice in which BALF was not collected. The tissue specimens were fixed in 4% paraformaldehyde for 48 h, gradient dehydrated, paraffin-embedded, and then cut into 4-μm thick sections, and stained with H&E.

BALF was collected by intratracheal injection of 1.0 mL of cold PBS after mice were sacrificed. BALF was collected by centrifugation at 4 °C 300g for 20 min into pellets, lysed erythrocytes, washed three times with cold PBS, and then centrifuged again and resuspended by counting the total number of cells in PBS. The protein concentration of untreated BLAF was determined using the BCA Protein Assay Kit (Beyotime, China).

2.10. Measurement of lung wet/dry (W/D) ratio and GSH, SOD, MDA, and MPO content in lung tissue

Lung tissue was collected after LPS treatment for 24 h, washed with saline, and blotted dry, weighed immediately to obtain the "wet" weight, and then oven-dried at 65 °C for 48 h to obtain the "dry" weight. Their ratio can indirectly reflect the edema within the lung tissue.

Lung tissues were homogenized and the levels of glutathione (GSH), superoxide dismutase (SOD), malondialdehyde (MDA), and myeloperoxidase (MPO) in the homogenate were measured using a kit (Nanjing Institute of Built-up Biological Engineering, Nanjing, China).

2.11. ELISA

Determination of cytokines in BALF or cell culture supernatants using ELISA. BALF was obtained from each sample separately, centrifuged, and the supernatant was collected. IL-1β, IL-6, and TNF-α protein levels were determined using ELISA kit (Nanjing Jiancheng Bioengineering Institute, China).

Moreover, RAW264.7 cells were cultured for 24 h, then pretreated with LPC 14:0 (20 μM) for 1 h. After adding LPS (1 μg/mL) to stimulate for 12 h, cell-free supernatants were collected to detect the secretion of IL - 1β, IL-6, and TNF-α, and the optical density at 450 nm was measured.

2.12. Western blot analysis

The wells of 10% polyacrylamide gels were loaded with 20ug of protein and sodium dodecyl sulfate-polyacrylamide gel electrophoresis (SDS-PAGE) was performed to separate the proteins. The proteins were then transferred to polyvinylidene difluoride (PVDF) membranes, which were closed in 5% skim milk for 1 h at room temperature. Next, the membrane was incubated with the primary antibody overnight at 4 °C, followed by three washes with TBST for 30 min, and then incubated with the Horseradish peroxidase (HRP)-conjugated secondary antibody for 1 h at room temperature. Detection of related protein expression: NLRP3, TXNIP, Caspase-1, IL-1β, and β-actin as the internal reference protein. Bands detection was performed using ECL (Amersham Pharmacia Biotech, Piscataway, NJ), and band intensities were quantified using Image lab gel analysis software.

2.13. Statistical analysis

Statistical analysis was performed using SPSS Statistics v18.0 (IBM, NY, USA). Differences among the three groups were analyzed using one-way ANOVA and multiple comparisons were performed using Tukey's method. Differences between the two groups were analyzed using a two-tailed paired Student's t-test. Non-normally distributed data use the rank sum test, Kruskal-Wallis H test, or Mann-Whitney *U* test. All data referenced above were presented as the means ± SEM. Statistical significance was defined as $*p < 0.05$.

3. Results

3.1. Demographic and clinical characteristics of participants

A total of 163 participants were eventually recruited, and the CAP

patients were divided into a discovery cohort (n = 31) and a validation cohort (n = 51). The participant design flowchart was shown in Fig. 1A.

Participants' demographic and clinical characteristics are shown in Table 1. Healthy controls and patients with CAP did not differ in gender ($p > 0.05$) and were younger in age than those with CAP ($p < 0.05$). There were no significant differences in age, gender, underlying diseases, and smoking history between patients with non-severe CAP and severe CAP ($p > 0.05$). Patients with severe CAP had significantly higher PSI, APACHE II, LOS, WBC, NE%, PCT, CRP, BUN, Scr, and LDH values than patients with non-severe CAP ($p < 0.05$), while they had lower PaO2/FiO2 and were more likely to be ventilated during their hospitalization than non-severe CAP patients ($p < 0.05$).

We compared the clinical parameters of CAP patients at two-time points on the 1st day of admission and before discharge and found that the clinical parameters WBC, NE%, CRP, PCT, and LDH all showed a significant downward trend in the remission stage ($p < 0.05$).

3.2. Untargeted metabolomics and multivariate data analysis

In the discovery cohort, plasma samples detected 2606 and 6392 spectral features by untargeted UHPLC-MS/MS analysis in the ESI + and ESI - modes, respectively. These obtained features were next analyzed using PCA and OPLS-DA. The QC is compactly aligned on the PCA plot, indicating stable instrument operation (Fig. S1A). PCA analysis revealed significant metabolic differences between acute and remission plasma samples, followed by OPLS-DA with a clearer distinction between the two groups (Fig. 1B and Fig. S1C). The R^2Y and Q^2 values (Table S1) showed that the OPLS-DA model was reliable with good fitting and predictive performance, and the key difference variables were found by its generated VIP values. 55 and 61 differential metabolites were identified in the non-severe CAP and severe CAP disease groups, respectively (Tables S2 and S3), mainly including fatty acyls, glycerophospholipids, sphingolipids, glycerolipids, steroids and steroid derivatives, etc., of which glycerophospholipids accounted for the majority, with 38 (69%) of non-severe CAP and 37 (61%) of severe CAP. The heatmap in Fig. 1C shows the relative intensities of the above differential metabolites in the acute phase and remission phase. It can be seen that most glycerophospholipid metabolites are up-regulated in the remission period. We speculate that such substances may have a protective effect in the disease process, so the analysis of glycerophospholipid metabolites is focused on in the validation phase.

In the validation cohort, the differential metabolites with repeated stable appearance and the same trend were further screened as candidate biomarkers by expanding the sample size. Untargeted metabolomics was still performed in the validation cohort, and 3333 and 4078 spectral features were detected in the ESI+ and ESI- modes, respectively. QCs were tightly clustered on the PCA plots (Fig. S1B), and the results of PCA and OPLS-DA are shown in Fig. S2A. Through the same screening conditions, 6 and 15 phospholipid differential metabolites were found in the two disease groups, respectively (Tables S4 and S5). Fig. 1D is the

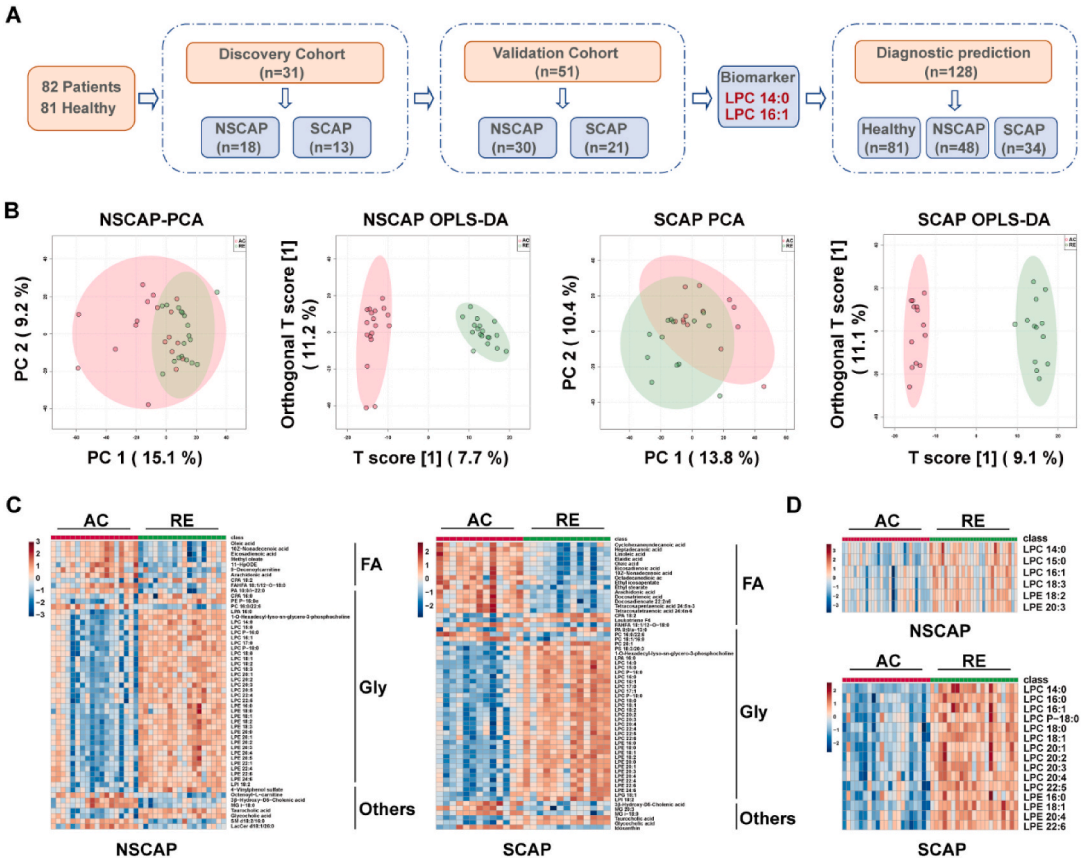

Fig. 1. Untargeted metabolomics and multivariate data analysis. (A) Study design. A total of 163 participants, including 48 non-severe CAP patients, 34 severe CAP patients, and 81 age- and sex-matched healthy volunteers, were divided into discovery and validation cohorts. (B) Plots of PCA scores and OPLS-DA scores comparing acute and remission plasma samples from CAP patients in the ESI- mode in the discovery cohort; shaded areas are the 95% confidence regions for each group. (C) Heatmap showing relative levels of differential metabolites in acute and remission plasma samples of CAP patients in the discovery cohort, with brown indicating higher relative levels of metabolites and blue indicating lower relative levels of metabolites. Heatmap (D) represents the relative intensities of differential metabolites in the two periods in the validation cohort. CAP community-acquired pneumonia, PCA principal component analysis, OPLS-DA orthogonal partial least squares discriminant analysis, NSCAP non-severe CAP, SCAP severe CAP, AC acute phase, RE remission phase, FA fatty acyls, Gly glycerophospholipids. (For interpretation of the references to color in this figure legend, the reader is referred to the Web version of this article.)

Table 1
Demographic and clinical characteristics of the 163 Participants enrolled in this study.

Characteristic	Discovery cohort (n = 31)		Validation cohort (n = 51)		Healthy (n = 81)
	NSCAP (n = 18)	SCAP (n = 13)	NSCAP (n = 30)	SCAP (n = 21)	
Age (years)	60.6 ± 9.59	65 ± 14.8	61.7 ± 12.1	66.0 ± 12.3	58.6 ± 8.8 *
Sex (male)	16 (88.9)	10 (76.9)	19 (64.3)	15 (71.4)	58 (71.6) **NS**
Hospital LOS (days)	10.2 ± 4.3	17.5 ± 9.3	8.1 ± 3.3	14.3 ± 9.6	NA
Underlying diseases					
Diabetes	4 (22.2)	5(38.5)	10 (33.3)	8 (38)	NA
Cardiovascular diseases	12 (66.7)	8(61.5)	11 (36.7)	8 (38)	NA
Cerebrovascular diseases	1 (5.6)	2(15.4)	0 (0)	1 (4.7)	NA
Chronic kidney disease	1 (5.6)	0(0)	3 (10)	2 (9.5)	NA
Immunodeficiency	1 (5.6)	0(0)	5 (16.7)	4 (19)	NA
Current smoker	11 (61.1)	6(46.2)	12 (40)	10 (47.6)	NA
PSI	10 ± 10.3	20.8 ± 11.2	13.3 ± 15.4	19.5 ± 12.8	NA
APACHE II	6.3 ± 3.7	12.2 ± 5.0	9.9 ± 4.8	16.3 ± 7.1	NA
Invasive ventilation	0 (0)	9 (69.2)	0 (0)	12 (57.1)	NA
Non-invasive ventilation	12 (66.7)	13 (100)	16 (53.3)	16 (76.2)	NA
PaO_2/FiO_2 (mmHg)	404.8 ± 43.1	169.2 ± 58.6	357.9 ± 32.2	196.2 ± 53.8	NA
WBC (3.5–9.5 X 10^9/L)	[a]9.1 ± 4.9	10.6 ± 3.6	8.7 ± 3.5	11.2 ± 6.2	NA
	[b]6.1 ± 1.6 *	7.3 ± 2.2 *	5.9 ± 2.1 ***	6.9 ± 4.7 ***	NA
NE (1.8–6.3 X 10^9/L)	[a]7.1 ± 4.4	8.4 ± 3.2	6.4 ± 3.0	10.7 ± 6.0	NA
	[b]3.7 ± 0.9 **	5.7 ± 2.6 **NS**	4.3 ± 2.0 ***	5.7 ±(2.2–17.5) ###	NA
CRP (0–8 mg/L)	[a]109.2 ± 58.5	171 (129.5–236.5)	108.0 (69.7–184.3)	185 (109.1–210.0)	NA
	[b]20.7 ± 20.5 ***	24.0 (16–52) ###	15.8 (6.9–35.5) ###	20.7 (6.6–52.3) ###	NA
PCT (0–0.5 ng/mL)	[a]0.17 (0.12–0.45)	8.5 (3.6–28.2)	0.36 (0.18–1.48)	4.3 (1.3–13.8)	NA
	[b]0.06 (0.03–0.08) ##	0.18 (0.13–0.28) ###	0.09 (0.05–0.20) ###	0.14 (0.1–1.4) ###	NA
BUN (35–80 Umol/L)	[a]70 (60–78.5)	89.4 ± 43.9	77 (57.3–94)	74.0 (57–129)	NA
	[b]66 (56–73.8) **NS**	70.9 ± 19.2 **NS**	63 (54.8–80) ##	72 (55.5–97.5) **NS**	NA
Scr (2.8–7.2 mmol/L)	[a]5.3 (4.5–6.1)	7.5 ± 3.2	6.8 (3.3–10.9)	9.3 ±(5–13.5)	NA
	[b]4.3 (3.9–5.7) #	4.7 ± 2.4 *	4.9 (4.1–6.8) **NS**	6.5 ±(3.4–11.9) **NS**	NA
LDH (0–247 u/L)	[a]278.9 ± 65.3	361 ± 119.1	306.7 ± 130.7	417 ±(279.5–583)	NA
	[b]226.9 ± 61.7 ***	276.5 ± 70.5 *	247.9 ± 70.8 *	282 ±(155.5–413.5) ***	NA

Qualitative data are presented as numbers (percentages) and quantitative data are presented as mean ± standard deviation or median (interquartile range).
CAP community-acquired pneumonia, NSCAP non-severe CAP, SCAP severe CAP, PSI Pneumonia Severity Index, APACHE II Acute Physiology and Chronic Health Evaluation II, LOS length of stay, PaO2/FiO2 ratio of arterial oxygen pressure to inspired oxygen concentration, WBC white blood cells, NE% neutrophil percentage, CRP C reactive protein, PCT Procalcitonin, BUN blood urea nitrogen, Scr serum creatinine, LDH lactate dehydrogenase.
* Two-tailed paired Student's t-test, # Mann Whitney *U* test, Qualitative unordered variables measured using the Fisher's exact test. Significance level, *$p < 0.05$, **$p < 0.01$, ***$p < 0.001$; NS not significant; all *p* values adjusted by Benjamini-Hochberg false discovery rate correction, adjusted *p-value* < 0.05 was considered statistically significant.
[a] Acute phase data.
[b] Remission phase data.

heatmap of the relative intensities of these differential metabolites during acute and remission phases. We ultimately screened for 6 and 14 differential metabolites, respectively (Tables S6 and S7), which were recurrent and trended consistently in the two cohort studies.

To test whether the OPLS-DA model has overfitting, the model was tested by imputing the data into SIMCA14 for 200 permutations, and the permutation test charts were obtained (Figs. S1D and S2B). It can be seen from the figures that all the replaced R^2Y and Q^2 values are below the original values. The slope of the regression line is large and the intercept with the left vertical axis is less than zero, which proves that there is no overfitting and that the results of the OPLS-DA model are reliable.

3.3. Quantification of metabolites and predictive performance for CAP

The screened differential metabolites were analyzed by the Venn diagram (Fig. 2A), then two common differential metabolites LPC 14:0 and LPC 16:1 were found in both disease groups, and their differences were significant. Therefore, we intend to further explore these two metabolites as potential biomarkers.

Then, the LPC 14:0 and LPC 16:1 content in human plasma samples was accurately determined by using a UHPLC-MS/MS targeted analysis method using the LPC 14:0 and LPC 16:0 standard. The results, as shown in the box-and-whisker plot in Fig. 2B, demonstrate that the concentration of LPC 14:0 and LPC 16:1 in the acute phase of the CAP patients was decreased compared with the healthy controls group, while their concentration in the recovery period after treatment increased and approached the level of healthy people, and the concentration of severe CAP disease group was lower than that of non-severe CAP disease group during the same period.

To investigate the diagnostic performance of these two metabolites, we performed correlation analysis and plotted the receiver operating characteristic (ROC) curves to assess their relationship with clinical features and the sensitivity and specificity for diagnosing CAP severity.

Clinical parameters (WBC, NE%, PCT, CRP, BUN, Scr, LDH) are commonly used indicators in the clinical treatment of CAP to judge disease severity and treatment effect. The correlation between the metabolites and clinical parameters was analyzed by Spearman correlation analysis (Fig. 2C), and correlation coefficient data were visible in Table S8. In the non-severe CAP disease group, LPC 14:0 was negatively correlated with CRP ($r = -0.430$, $p < 0.001$) and PCT ($r = -0.511$, $p < 0.001$), but not with WBC, NE%, BUN, Scr, and LDH. LPC16:1 has a weak negative correlation with CRP ($r = -0.309$, $p = 0.002$) and PCT ($r = -0.404$, $p < 0.001$), and has no correlation with other clinical parameters. In the severe CAP disease group, LPC 14:0 had a negative correlation with WBC ($r = -0.304$, $p = 0.012$), NE% ($r = -0.356$, $p = 0.0029$), CRP ($r = -0.532$, $p < 0.001$) and PCT ($r = -0.461$, $p < 0.001$), no correlation with Scr, LDH and BUN. LPC16:1 has a weak negative correlation with CRP ($r = -0.479$, $p < 0.001$) and PCT ($r = -0.420$, $p < 0.001$), no correlation with other parameters.

The area under the curve (AUC), specificity, and sensitivity of the ROC curve was used to evaluate the performance of these two metabolites in predicting CAP severity. As shown in Fig. 2D, the performance of LPC 14:0 in diagnosing non-severe CAP with an AUC value of 0.855,

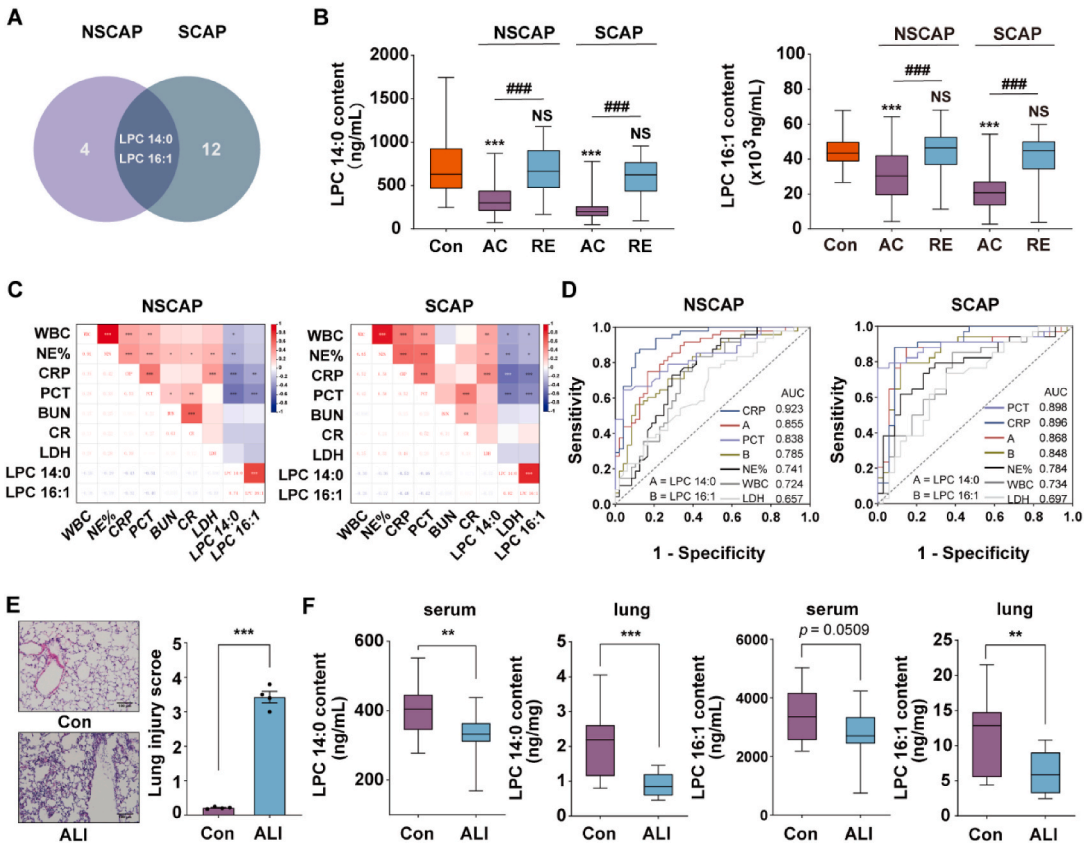

Fig. 2. Quantification of metabolites and predictive performance for CAP (A) Venn diagram: showing differential metabolites common to non-severe CAP and severe CAP disease groups. (B) Box-and-whisker plots of metabolites LPC 14:0 and LPC 16:1concentrations in CAP patients and healthy controls. The horizontal line represents the median; the bottom and the top of the box represent the bottom quartile and upper quartile; the whiskers represent the minimum and maximum values. (C) Spearman's correlations heatmap of biomarkers LPC 14:0, LPC 16:1, and clinical parameters. Red and blue indicate positive and negative correlations, respectively, and the darker the color, the stronger the correlation. (D) ROC curve analysis of the predictive performance of LPC 14:0, LPC 16:1, and various clinical parameters in non-severe CAP and severe CAP disease, respectively. (E) Evaluation of lung injury by H & E staining of lung tissue (Bar = 100 μm, magnification × 200) and the lung injury score. (F) Concentrations of LPC14:0 in serum and lung of control and ALI mice. * vs control, # AC vs RE, $*p < 0.05$, $**p < 0.01$, $***p < 0.001$. CAP community-acquired pneumonia, NSCAP non-severe CAP, SCAP severe CAP, AC acute phase, RE remission phase. (For interpretation of the references to color in this figure legend, the reader is referred to the Web version of this article.)

sensitivity 0.750, specificity 0.833, significant $p < 0.001$. The AUC value of LPC16:1 is 0.785, sensitivity 0.563, specificity 0.896, and significance $p < 0.001$. In predicting severe CAP, the AUC value of LPC 14:0 is 0.868, with 0.882 sensitivity and 0.853 specificity, significant $p < 0.001$. The AUC values of LPC16:1 is 0.848, sensitivity 0.794, specificity 0.882, and the significance $p < 0.001$. We also analyzed the diagnostic performance of CRP, PCT, WB, NE%, and LDH, and the data are shown in Table S9. Compared with these clinical parameters, LPC 14:0 and LPC16:1 performed better than WB, NE%, and LDH, and slightly worse than CRP, and PCT.

Through the above results, we found that the correlation and predictive performance of LPC 14:0 for CAP was better than that of LPC 16:1. Meanwhile, we used LPS to establish an ALI model in mice (Fig. 2E) and then detected these two lipids in ALI mice using target MS assay, and we found that the level of LPC14:0 in serum and lung tissue was significantly lower than that of the normal control mice, while LPC 16:1 was only found lower in lung tissue. The trend of LPC14:0 in animals was substantially consistent with that in humans (Fig. 2F). These results indicated that LPC 14:0 can be used as a potential biomarker and therapeutic target for CAP; therefore, this lipid was selected for subsequent in vitro and in vivo experiments.

3.4. LPC 14:0 pretreatment attenuates LPS-induced oxidative damage in RAW 264.7 cells

We first investigated whether LPC 14:0 pretreatment can protect RAW 264.7 cells from LPS-induced oxidative stress. Firstly, CCK-8 observed the effect of different doses of LPS and LPC 14:0 on cell viability. The results showed that LPS was completely non-toxic to cells in the dose range of 0.1–20 μg/mL. LPS can promote cell proliferation in the dose range of 0.1–1 μg/mL, so 20 μg/mL was used in the apoptosis experiment (Fig. 3A). LPC 14:0, either single or combined with LPS (1 μg/ml), was non-toxic in the 0–20 μM range (Fig. 3B).

LPS stimulated RAW 264.7 to generate ROS and triggered oxidative stress, which resulted in oxidative damage to cells, while LPC 14:0 pretreatment could reduce the rate of apoptosis in cells (Fig. 3C and D). We further studied the antioxidant effect of LPC 14:0. The results showed that LPC 14:0 pretreatment could effectively reduce the generation of ROS (Fig. 3E and F), depletion of antioxidant enzymes (SOD, GSH) (Fig. 3G and H).

3.5. LPC 14:0 inhibits LPS-induced inflammatory response and NLRP3 inflammasome activation in RAW 264.7 cells

We continued to investigate the effect of LPC14:0 on the inflammatory response of LPS-induced RAW264.7 cells. We found that stimulating RAW 264.7 cells with LPS alone promoted the secretion of IL-1β,

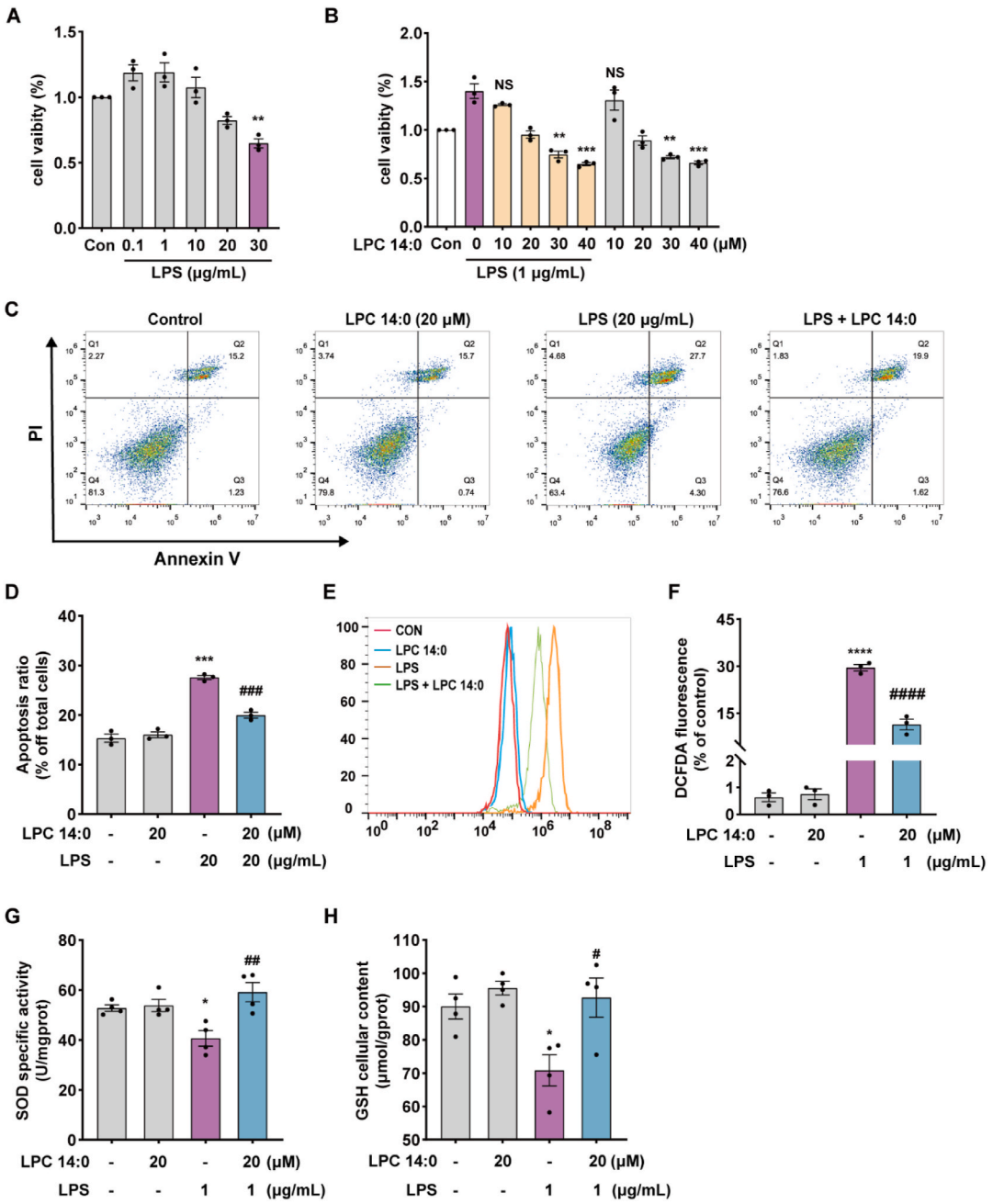

Fig. 3. LPC 14:0 pretreatment attenuates LPS-induced oxidative damage in RAW 264.7 cells. RAW 264.7 cells were subjected to various concentrations of LPS (0.1, 1, 10, 20, 30 μg/mL) for 12h. (A) Cell viability after LPS-only exposure was measured by CCK8 assay. RAW 264.7 cells were pretreated with different concentrations of LPC 14:0 (10 μM, 20 μM, 30 μM, 40 μM) for 1 h, and then LPS (1 μg/mL) was added for 12 h. (B) Cell viability after LPS + LPC 14:0 or LPC 14:0 only exposure was measured by CCK8 assay. RAW 264.7 cells were pretreated with LPC 14:0 (20 μM) for 1 h, and then LPS (20 μg/mL) was added for 12 h. After collecting cells, add 5 μl FITC Annexin V and 5 μl PI and incubate for 15 min at room temperature in the dark. (C, D) The effect of LPC 14:0 on LPS-induced apoptosis was detected by flow cytometry. RAW 264.7 cells were pretreated with LPC 14:0 (20 μM) for 1 h, and then LPS (1 μg/mL) was added for 12 h. Cells were harvested and resuspended in 1 ml of serum-free medium containing 1 μl of DCFH-DA, incubated at 37 °C in the dark for 20 min, and washed with cold PBS three times. (E, F) ROS levels were detected by flow cytometry. (G, H) Commercial SOD and GSH kits were used to detect the effects of LPC 14:0 pretreatment on LPS-stimulated SOD and GSH. All data are presented as mean ± SEM (n = three or four times independent experiments). * vs control group, # vs LPS group, $*p < 0.05$, $**p < 0.01$, $***p < 0.001$.

IL-6, and TNF-α, while LPC14:0 suppressed the above-mentioned inflammatory factors (Fig. 4A–C). Since LPC 14:0 was found to effectively reduce LPS-induced ROS generation in RAW 264.7 cells, and ROS could stimulate the activation of TXNIP and then promote the activation of the NLRP3 inflammasome, we went on to investigate whether LPC14:0 could block LPS-induced NLRP3 inflammasome activation in RAW 264.7 cells. The results suggested that LPC 14:0 treatment could significantly inhibit the LPS-induced expression of NLRP3, TXNIP, Caspase-1, and IL-1β proteins (Fig. 4D–K).

3.6. LPC 14:0 treatment alleviates LPS-induced ALI in mice

Based on these in vitro experimental results, we further investigated whether LPC14:0 treatment has a protective effect on ALI in mice. As shown in Fig. 5A, the LPS-treated group showed obvious pathological changes in lung tissue, including accumulation of inflammatory cells in the alveoli, intra-alveolar hemorrhage, and thickening of the alveolar wall. However, these changes were significantly attenuated by LPC 14:0 pretreatment. Also, the LPC 14:0 treatment reduced lung injury scores

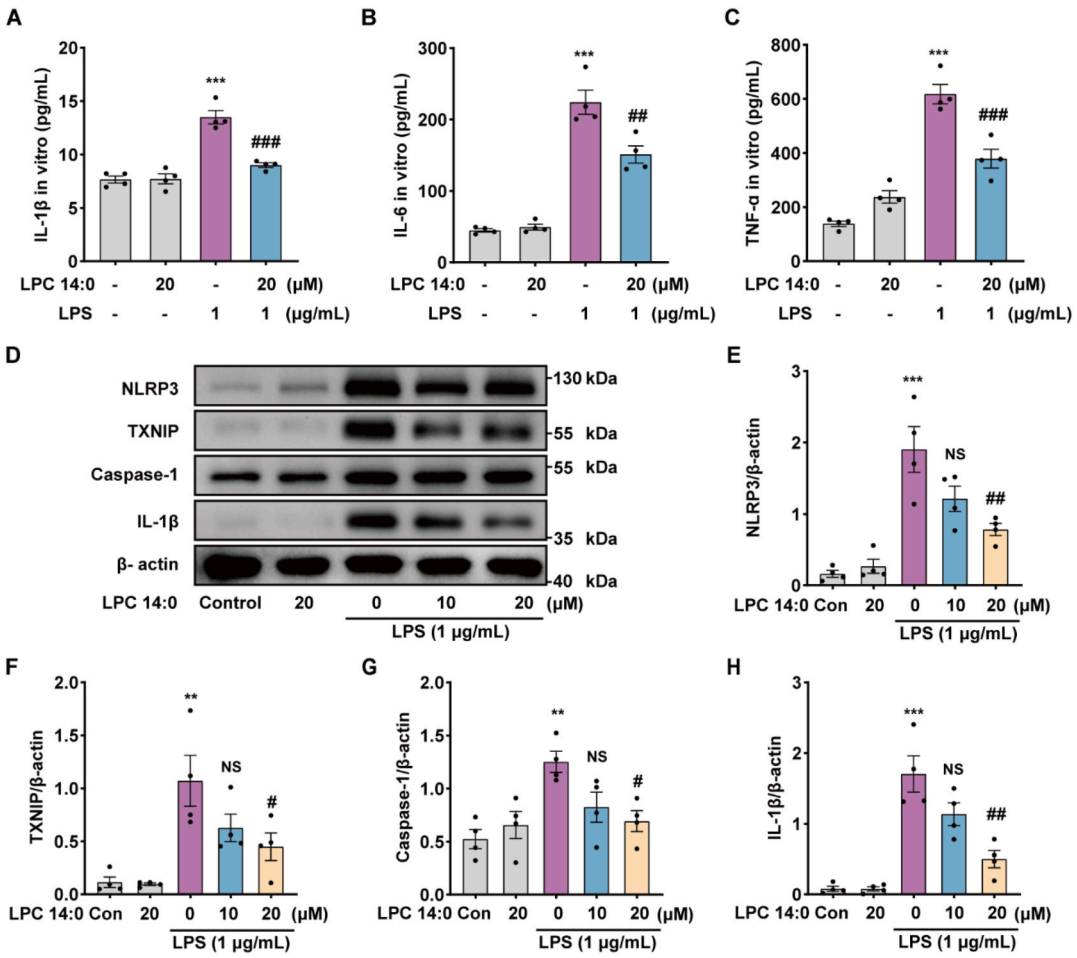

Fig. 4. LPC 14:0 inhibits LPS-induced inflammatory response and NLRP3 inflammasome activation in RAW 264.7 cells. RAW 264.7 cells were pretreated with LPC14:0 (20 μM) for 1 h, and then stimulated by LPS (1 μg/mL) for 12 h, and the cells and cell supernatants were collected. (A–C) ELISA kits were used to measure the levels of IL-1β, IL-6, and TNF-α in cell supernatants. (D) Western blot was performed to detect the protein expressions of NLRP3, TXNIP, Caspase-1, and IL-1β after protein extraction from cells. (E–H) The protein expression was quantified with β-actin as an internal reference. All data are presented as mean ± SEM (n = four times independent experiments). * vs control group, # vs LPS group, $^{*}p < 0.05$, $^{**}p < 0.01$, $^{***}p < 0.001$.

compared to the LPS-treated group (Fig. 5B). We determined the degree of pulmonary edema in mice by the lung W/D ratio and protein leakage in BALF. As shown in Fig. 5C and D, the lung W/D ratio and protein concentration in LPS-stimulated mice were dramatically higher than those in the control and LPC 14:0-treated groups alone, while LPC 14:0 pretreatment significantly alleviated these inflammatory changes. In addition, stimulation of LPS resulted in inflammatory cell aggregation in BALF of mice, which could be effectively inhibited by LPC 14:0 pretreatment (Fig. 5E). As illustrated in Fig. 5F, LPC 14:0 pretreatment effectively suppressed the LPS-induced increase in MPO activity, which is an indicator of neutrophil accumulation within the lung.

3.7. LPC 14:0 treatment inhibits LPS-stimulated inflammation response, oxidative stress, and NLRP3 inflammasome activation in ALI mice

To observe the effect of LPC14:0 on the inflammatory response and oxidative stress induced by LPS in mice, we detected the secretion levels of inflammatory factors IL-1β, IL-6, and TNF-α in mouse BALF and the contents of GSH, SOD, and MDA in lung tissue homogenates. Our results showed that, in addition to IL-6, LPC 14:0 pretreatment not only effectively downregulated the generation of IL-1β, TNF-α, and MDA but also significantly attenuated the depletion of SOD and GSH (Fig. 6A–F), both of which antioxidative enzymes have a major function in suppressing LPS-induced oxidative stress. In vitro cell experiments, we found that LPC14:0 effectively reduced the activation of LPS-induced NLRP3 inflammasome. Therefore, this study further explored whether LPC14:0 could block the activation of NLRP3 inflammatory bodies in vivo. The results showed that LPS stimulation could significantly promote the expression of NLRP3, TXNIP, Caspase-1, and IL-1β proteins, while LPC 14:0 pretreatment could significantly attenuate this effect (Fig. 6G–K).

4. Discussion

In this study, we observed significant differences in metabolomic profiles between plasma samples from the acute phase and remission phase in CAP. Through the metabolomic analysis of the discovery set and the validation set, we found that lysophosphatidylcholines (LPCs) were the most dominant differential metabolites and subsequently identified that LPC 14:0 is a key metabolite for recovery in CAP patients and has good performance in predicting the severity of CAP. We then observed the protective effect of LPC 14:0 in a mouse ALI model, with similar pathological features to human ALI [26], and in the ARW 264.7 cellular inflammation model.

Some previous reports have mentioned that in some inflammatory diseases with examples of CAP [27], bacteremia [28], septicemia [29], and septic shock [30], a decrease in the concentration of serum phospholipids (PCs, LPCs, LPEs) has been recorded. In particular, recent studies by Müller [31], Arshad H [32], and others have found that the serum LPCs concentration of CAP patients decreased significantly on admission and returned to normal during the recovery period, which is

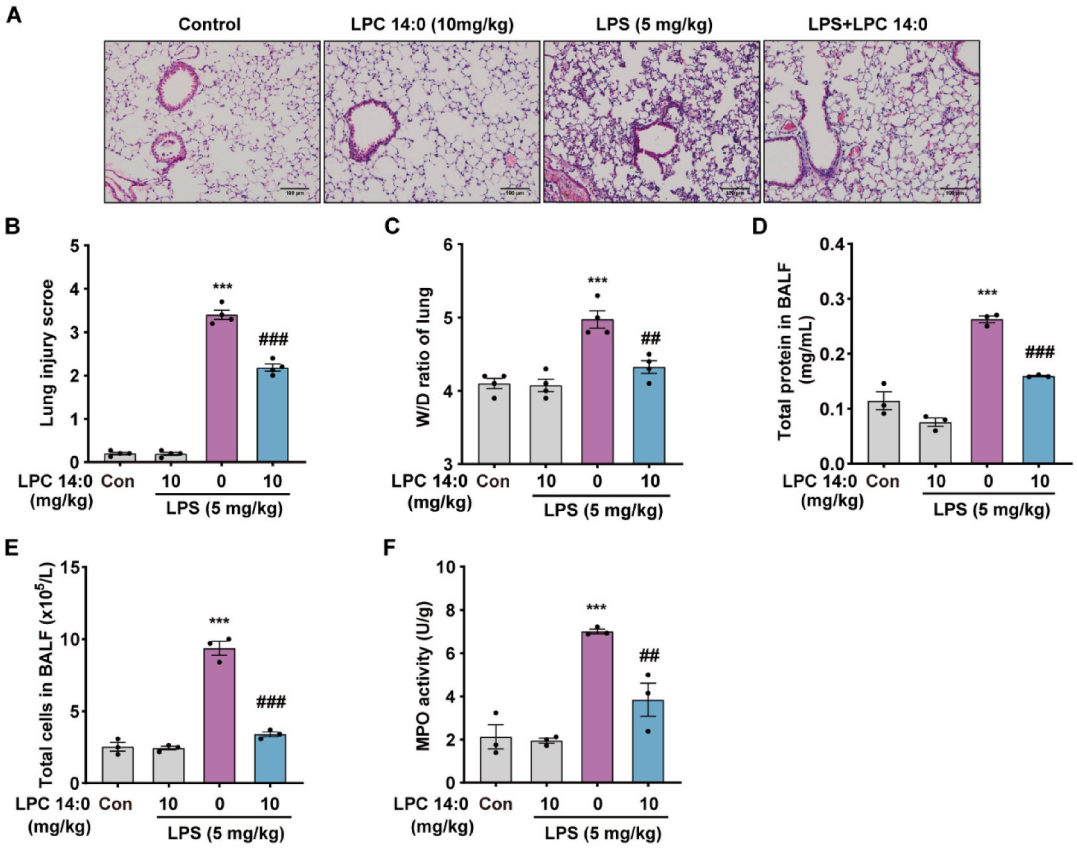

Fig. 5. Protective effect of LPC 14:0 treatment on LPS-induced ALI in mice. LPC 14:0 (10 mg/kg) was pre-administered by subcutaneous injection 2 h before intratracheal infusion of LPS (5 mg/kg) and administered again 12 h later. Lung tissue and BLFA were collected 24 h after LPS treatment. (A) Evaluation of lung injury by H & E staining of lung tissue (Bar = 100 μm, magnification × 200). (B) The lung injury score was mainly based on the following variables: alveolar and interstitial edema, inflammatory cell infiltration, and hemorrhage. Severity was scored on a 0–4 scale: no injury = 0; 25% injury = 1; 50% injury = 2; 75% injury = 3; diffuse injury = 4. Each sample has three sections, which were observed and photographed under an optical microscope. Five fields of view were selected from each section and randomly analyzed by pathologists, and the average value was used as the sample score. (C) The W/D ratio was determined in lung tissue. (D–E) Measurement of protein content and cell number in BALF. (F) The activity of MPO in lung tissue was determined using a kit. All data are presented as mean ± SEM (n = 3–4 per group). * vs control group, # vs LPS group, $*p < 0.05$, $**p < 0.01$, $***p < 0.001$.

consistent with our results.

PCs and LPCs are indispensable ingredients that make up human cell membranes and lung surface active substances [33], both of which are essential in lung formation. PCs in the lungs are mainly synthesized by alveolar type II cells [34], which can be decomposed by phospholipase A2 (PLA2) into fatty acids and LPCs, and LPCs will eventually be hydrolyzed into another free fatty acid [32]. The reduction of PCs and LPCs in the lung tissue of CAP patients may reflect the damage of alveolar epithelial cells and their loss of function, which in turn will inevitably lead to the dysfunction of cell membranes and pulmonary surfactant, further aggravating the damage of lung tissue.

The pro-inflammatory and anti-inflammatory effects of LPCs in a variety of diseases have attracted widespread attention. Earlier studies have found that the effect of LPCs on inflammation correlates with their acyl chain length and degree of saturation. Saturated LPCs, such as LP16:0, are a proven mediator of inflammation and can induce inflammatory responses. While polyunsaturated acyl LPCs, including LPC (18:0, 18:1, 20:4, and 22:6), act as anti-inflammatory lipid mediators, reduce plasma leakage and inflammatory cell activation, and inhibit inflammatory mediators (IL-1β, IL-6, TNF-α, NO, etc.) production [35,36]. Therefore, different LPCs play different roles in the regulation of inflammation. Recent studies have shown that stearoyl lysophosphatidylcholine (LPC 18:0) [25,37,38] can control inflammation by inhibiting the release of HMGB1 through the G2A-CaMKKβ-AMPK pathway. Palmitoyl lysophosphatidylcholine (LPC 16:0) promotes IL-1β secretion and foam cell formation from human monocytes and endothelial cells through an NLRP3 inflammasome-mediated pathway [39]. In addition, it has been reported that LPCs can effectively control the growth of Mycobacterium tuberculosis (Mtb) by inhibiting the production of inflammatory cytokines and promoting phagocytic maturation through cAMP-activated PKA-PI3K–P38MAPK signaling pathway in macrophages infected with Mycobacterium tuberculosis [40].

Other than previous studies of LPC 14:0, which are closely associated with rapid increases in obesity in infancy and childhood [41], except for few reports on the role of LPC14:0 in inflammation. We identified LPC 14:0 in a metabolome study of acute and remission plasma samples from CAP patients, and based on its features of down-regulation in the acute phase and up-regulated in the remission phase, we speculate that the metabolite LPC 14:0 has a recovery-promoting effect on CAP. Oxidative stress and inflammatory response have mutually reinforcing roles in the pathogenesis of inflammatory diseases [14]. Oxidative stress can promote the expression of pro-inflammatory factors, while inflammation can likewise stimulate the overproduction of ROS to induce oxidative stress [42]. Our findings provide the first evidence that LPC 14:0 protects against LPS-induced ALI in mice by inhibiting inflammatory responses and oxidative stress, which is heavily reliant on inhibiting the LPS-activated TXNIP-NLRP3 inflammatory signaling pathway. This result suggests that LPC 14:0 may be a valuable drug candidate for the treatment of inflammatory diseases such as CAP.

Although our results are very consistent with the published literature, this study suffers from several limitations, mainly the absence of an external independent sample validation and the small sample size. Since

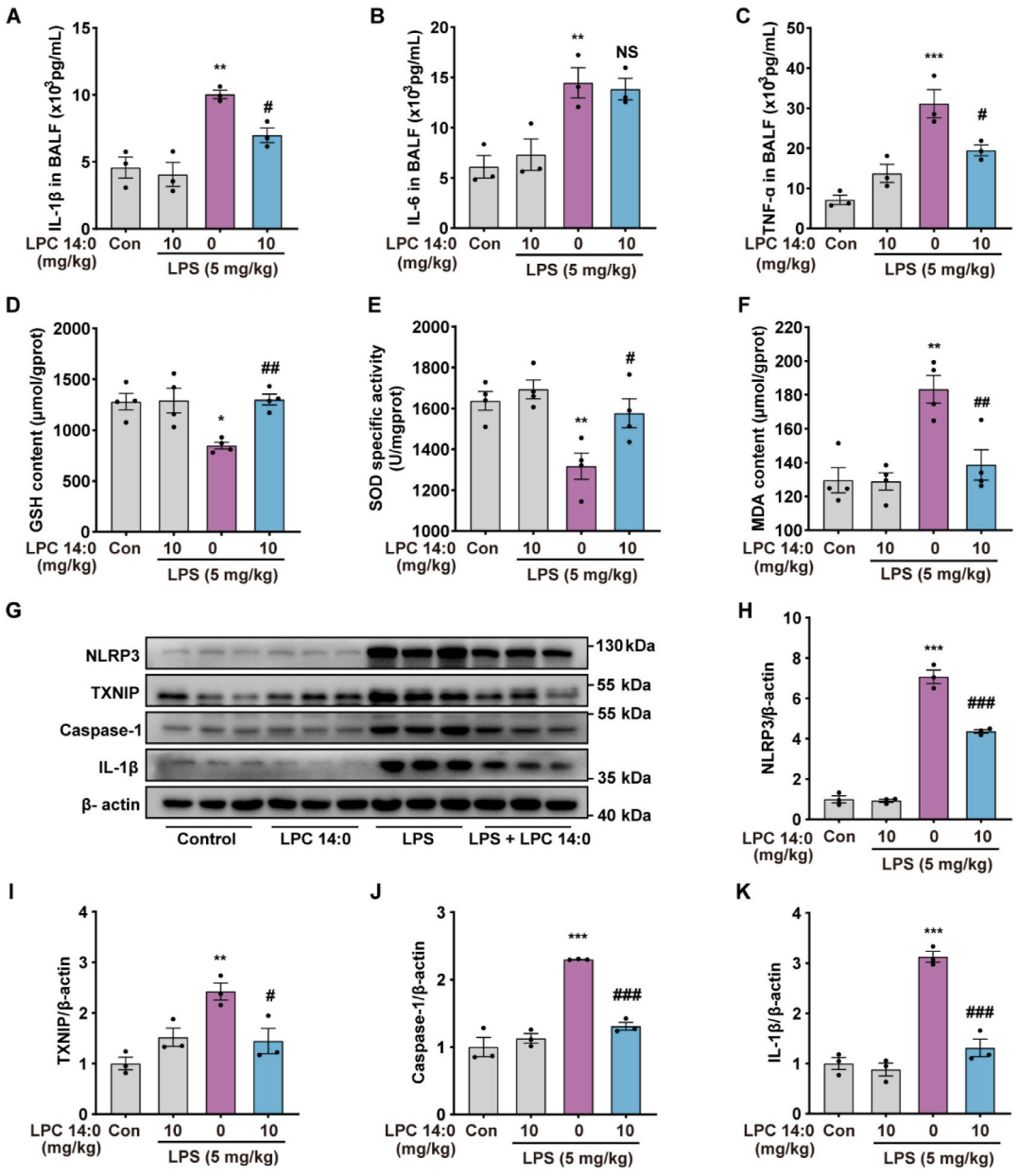

Fig. 6. LPC 14:0 treatment inhibits inflammation response, oxidative stress, and activation of the NLRP3 inflammasome in LPS-induced ALI mice. LPC 14:0 (10 mg/kg) was pre-administered by subcutaneous injection 2 h before intratracheal infusion of LPS (5 mg/kg) and administered again 12 h later. Lung tissue and BLFA were collected 24 h after LPS treatment. (A–C) The levels of IL-1β, IL-6, and TNF-α in BLAF were detected by ELISA. (D–F) The contents of GSH, SOD, and MDA in lung tissue homogenates were determined using commercial kits. (G) Proteins were extracted from lung tissue, and the expression of NLRP3, Txnip, Caspase-1, and IL-1β proteins were detected by Western blotting with specific antibodies. (H–K) Quantification of protein expression with β-actin as an internal control. All data are presented as mean ± SEM (n = 3–4 per group). * vs control group, # vs LPS group, $*p < 0.05$, $**p < 0.01$, $***p < 0.001$.

this is a controlled paired study, interference from small samples is minimized. In addition, the present experiment did not investigate the mechanism of action of how LPC 14:0 reduces the NLRP3 inflammasome. Previous studies have found that immune cells stimulated by LPS can bind to TLR4 on the cell membrane to activate NF-κB, and activated NF-κB can increase the expression of NLRP3 and pro-IL-1β at the transcriptional level, which is the initiation signal for NLRP3 inflammatory vesicles. We will continue to investigate the mechanism of action of LPC 14:0 on the classical inflammatory pathway NF-κB and explore whether it is related to the antioxidant pathway Nrf2 [43,44]. Therefore, the promising biomarker need to be studied in greater depth before it can be applied to the clinic.

5. Conclusions

Our results demonstrate that LC-MS/MS-based metabolomics approaches can serve to reveal metabolic changes in CAP and to build metabolite profiles that correlate with disease severity. LPC14:0 has the potential to become a new biomarker for predicting CAP severity. In addition, we validated LPC 14:0 may be a potential therapeutic target to improve the clinical efficacy of CAP in animal and cellular models by inhibiting the TXNIP-NLRP3 inflammatory signaling pathway (Fig. 7).

Declaration of conflicts of interest

The authors declare no competing conflicts of interest.

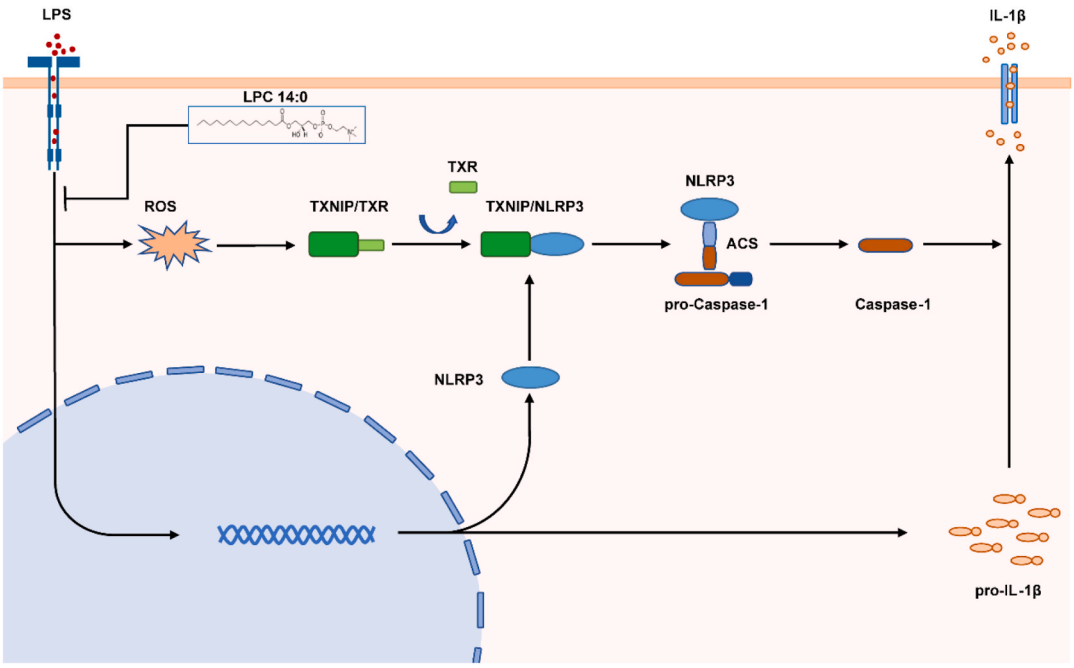

Fig. 7. Scheme of the mechanisms in the protective effect of LPC 14:0 on LPS-induced ALI. LPS can promote the production of ROS, which activates the separation of TXNIP from TRX and then binds to NLRP3, leading to activation of the NLRP3 inflammasome, which will release a large number of mature inflammatory factors IL-1β. LPC 14:0 treatment significantly protected LPS-induced ALI by inhibiting oxidative stress and inflammation damage, which is largely dependent on suppressing LPS-activated TXNIP/NLRP3 inflammasome.

Funding

This work was supported by the Project of the National Natural Science Foundation of China (81970066).

Authors' contributions

Design of the study: Yuping Li Hongchang Gao, Clinical Sample Collection: Huizhen Wu, Xiong Lei, Metabolomics and statistical analysis of data: Fen Xiong, Wengang Nan, Cong Lou, Hong Zheng, Chen Li, Animal, and cellular experiments and statistical analysis of data: Wengang Nan, Manuscript writing: Wengang Nan, Fen Xiong; Final approval of manuscript: All authors.

Declaration of competing interest

We declare that we do not have any commercial or associative interest that represents a conflict of interest in connection with the work submitted.

Data availability

The data that has been used is confidential.

Acknowledgments

We would like to thank all participants for collecting the data for this clinical study.

Appendix A. Supplementary data

Supplementary data to this article can be found online at https://doi.org/10.1016/j.redox.2022.102556.

References

[1] A. Torres, P. Ramirez, B. Montull, et al., Biomarkers and community-acquired pneumonia: tailoring management with biological data[C]//Seminars in respiratory and critical care medicine, Thieme Med. Publish 33 (3) (2012) 266–271.
[2] M. Christ-Crain, S.M. Opal, Clinical review: the role of biomarkers in the diagnosis and management of community-acquired pneumonia[J], Crit. Care 14 (1) (2010) 1–11.
[3] B. Cao, Y. Huang, D.Y. She, et al., Diagnosis and treatment of community-acquired pneumonia in adults: 2016 clinical practice guidelines by the Chinese Thoracic Society, Chinese Medical Association[J], clinic. respir. J. 12 (4) (2018) 1320–1360.
[4] S. Aliberti, A.M. Brambilla, J.D. Chalmers, et al., Phenotyping community-acquired pneumonia according to the presence of acute respiratory failure and severe sepsis [J], Respir. Res. 15 (1) (2014) 1–10.
[5] M.F. Di Pasquale, G. Sotgiu, A. Gramegna, et al., Prevalence and etiology of community-acquired pneumonia in immunocompromised patients[J], Clin. Infect. Dis. 68 (9) (2019) 1482–1493.
[6] C.W. Lanks, A.I. Musani, D.W. Hsia, Community-acquired pneumonia and hospital-acquired pneumonia[J], Med. Clinics 103 (3) (2019) 487–501.
[7] D.S. Wishart, Metabolomics for investigating physiological and pathophysiological processes[J], Physiol. Rev. 99 (4) (2019) 1819–1875.
[8] N.J. Serkova, T.J. Standiford, K.A. Stringer, The emerging field of quantitative blood metabolomics for biomarker discovery in critical illnesses[J], Am. J. Respir. Crit. Care Med. 184 (6) (2011) 647–655.
[9] B.P. Scicluna, P.M.C. Klein Klouwenberg, L.A. van Vught, et al., A molecular biomarker to diagnose community-acquired pneumonia on intensive care unit admission[J], Am. J. Respir. Crit. Care Med. 192 (7) (2015) 826–835.
[10] K.K.W. To, K.C. Lee, S.S.Y. Wong, et al., Lipid metabolites as potential diagnostic and prognostic biomarkers for acute community acquired pneumonia[J], Diagn. Microbiol. Infect. Dis. 85 (2) (2016) 249–254.
[11] P. Ning, Y. Zheng, Q. Luo, et al., Metabolic profiles in community-acquired pneumonia: developing assessment tools for disease severity[J], Crit. Care 22 (1) (2018) 1–14.
[12] T.W. Stief, O. Ijagha, B. Weiste, et al., Analysis of hemostasis alterations in sepsis [J], Blood Coagul. Fibrinolysis 18 (2) (2007) 179–186.
[13] H. Chen, C. Bai, X. Wang, The value of the lipopolysaccharide-induced acute lung injury model in respiratory medicine[J], Expet Rev. Respir. Med. 4 (6) (2010) 773–783.
[14] H. Lv, Q. Liu, Z. Wen, et al., Xanthohumol ameliorates lipopolysaccharide (LPS)-induced acute lung injury via induction of AMPK/GSK3β-Nrf2 signal axis[J], Redox Biol. 12 (2017) 311–324.
[15] C.H. Huang, M.L. Yang, C.H. Tsai, et al., Ginkgo biloba leaves extract (EGb 761) attenuates lipopolysaccharide-induced acute lung injury via inhibition of oxidative stress and NF-κB-dependent matrix metalloproteinase-9 pathway[J], Phytomedicine 20 (3–4) (2013) 303–309.

[16] X. Han, Y.C. Wu, M. Meng, et al., Linarin prevents LPS-induced acute lung injury by suppressing oxidative stress and inflammation via inhibition of TXNIP/NLRP3 and NF-κB pathways[J], Int. J. Mol. Med. 42 (3) (2018) 1460–1472.
[17] X.Q. Ding, W.Y. Wu, R.Q. Jiao, et al., Curcumin and allopurinol ameliorate fructose-induced hepatic inflammation in rats via miR-200a-mediated TXNIP/NLRP3 inflammasome inhibition[J], Pharmacol. Res. 137 (2018) 64–75.
[18] Y. Liu, G. Lou, A. Li, et al., AMSC-derived exosomes alleviate lipopolysaccharide/d-galactosamine-induced acute liver failure by miR-17-mediated reduction of TXNIP/NLRP3 inflammasome activation in macrophages[J], EBioMedicine 36 (2018) 140–150.
[19] X.T. Huang, W. Liu, Y. Zhou, et al., Galectin-1 ameliorates lipopolysaccharide-induced acute lung injury via AMPK-Nrf2 pathway in mice[J], Free Radic. Biol. Med. 146 (2020) 222–233.
[20] Y. He, H. Hara, G. Núñez, Mechanism and regulation of NLRP3 inflammasome activation[J], Trends Biochem. Sci. 41 (12) (2016) 1012–1021.
[21] R. Zhou, A. Tardivel, B. Thorens, et al., Thioredoxin-interacting protein links oxidative stress to inflammasome activation[J], Nat. Immunol. 11 (2) (2010) 136–140.
[22] B. Cao, Y. Huang, D.Y. She, et al., Diagnosis and treatment of community-acquired pneumonia in adults: 2016 clinical practice guidelines by the Chinese Thoracic Society, Chinese Medical Association[J], clinic. respir. J. 12 (4) (2018) 1320–1360.
[23] F. Xiong, K. Gong, H. Xu, et al., Optimized integration of metabolomics and lipidomics reveals brain region-specific changes of oxidative stress and neuroinflammation in type 1 diabetic mice with cognitive decline[J], J. Adv. Res. (2022), https://doi.org/10.1016/j.jare.2022.02.011.
[24] J.J. Yan, J.S. Jung, J.E. Lee, et al., Therapeutic effects of lysophosphatidylcholine in experimental sepsis[J], Nat. Med. 10 (2) (2004) 161–167.
[25] H. Quan, H.B. Bae, Y.H. Hur, et al., Stearoyl lysophosphatidylcholine inhibits LPS-induced extracellular release of HMGB1 through the G2A/calcium/CaMKKβ/AMPK pathway[J], Eur. J. Pharmacol. 852 (2019) 125–133.
[26] M. Rojas, C.R. Woods, A.L. Mora, et al., Endotoxin-induced lung injury in mice: structural, functional, and biochemical responses[J], Am. J. Physiol. Lung Cell Mol. Physiol. 288 (2) (2005) L333–L341.
[27] W.H. Cho, H.J. Yeo, S.H. Yoon, et al., Lysophosphatidylcholine as a prognostic marker in community-acquired pneumonia requiring hospitalization: a pilot study [J], Eur. J. Clin. Microbiol. Infect. Dis. 34 (2) (2015) 309–315.
[28] M.M. Banoei, H.J. Vogel, A.M. Weljie, et al., Plasma lipid profiling for the prognosis of 90-day mortality, in-hospital mortality, ICU admission, and severity in bacterial community-acquired pneumonia (CAP)[J], Crit. Care 24 (1) (2020) 1–16.
[29] W. Drobnik, G. Liebisch, F.X. Audebert, et al., Plasma ceramide and lysophosphatidylcholine inversely correlate with mortality in sepsis patients[J], J. Lipid Res. 44 (4) (2003) 754–761.
[30] M. Ferrario, A. Cambiaghi, L. Brunelli, et al., Mortality prediction in patients with severe septic shock: a pilot study using a target metabolomics approach[J], Sci. Rep. 6 (1) (2016) 1–11.
[31] D.C. Müller, A. Kauppi, A. Edin, et al., Phospholipid levels in blood during community-acquired pneumonia[J], PLoS One 14 (5) (2019), e0216379.
[32] H. Arshad, J.C.L. Alfonso, R. Franke, et al., Decreased plasma phospholipid concentrations and increased acid sphingomyelinase activity are accurate biomarkers for community-acquired pneumonia[J], J. Transl. Med. 17 (1) (2019) 1–18.
[33] D.L. Poelma, M.R. Ju, S.C. Bakker, et al., A common pathway for the uptake of surfactant lipids by alveolar cells[J], Am. J. Respir. Cell Mol. Biol. 30 (5) (2004) 751–758.
[34] R. Schmidt, U. Meier, M. Yabut-Perez, et al., Alteration of fatty acid profiles in different pulmonary surfactant phospholipids in acute respiratory distress syndrome and severe pneumonia[J], Am. J. Respir. Crit. Care Med. 163 (1) (2001) 95–100.
[35] P. Liu, W. Zhu, C. Chen, et al., The mechanisms of lysophosphatidylcholine in the development of diseases[J], Life Sci. 247 (2020), 117443.
[36] S.H. Law, M.L. Chan, G.K. Marathe, et al., An updated review of lysophosphatidylcholine metabolism in human diseases[J], Int. J. Mol. Sci. 20 (5) (2019) 1149.
[37] J.M. Kim, H.J. Han, Y.H. Hur, et al., Stearoyl lysophosphatidylcholine prevents lipopolysaccharide-induced extracellular release of high mobility group box-1 through AMP-activated protein kinase activation[J], Int. Immunopharm. 28 (1) (2015) 540–545.
[38] W. Li, W. Zhang, M. Deng, et al., Stearoyl lysophosphatidylcholine inhibits endotoxin-induced caspase-11 activation[J], Shock 50 (3) (2018) 339.
[39] R. Corrêa, L.F.F. Silva, D.J.S. Ribeiro, et al., Lysophosphatidylcholine induces NLRP3 inflammasome-mediated foam cell formation and pyroptosis in human monocytes and endothelial cells[J], Front. Immunol. (2020) 2927.
[40] H.J. Lee, H.J. Ko, D.K. Song, et al., Lysophosphatidylcholine promotes phagosome maturation and regulates inflammatory mediator production through the protein kinase a–phosphatidylinositol 3 kinase–p38 mitogen-activated protein kinase signaling pathway during mycobacterium tuberculosis infection in mouse macrophages[J], Front. Immunol. 9 (2018) 920.
[41] P. Rzehak, C. Hellmuth, O. Uhl, et al., Rapid growth and childhood obesity are strongly associated with lysoPC (14: 0)[J], Ann. Nutr. Metabol. 64 (3–4) (2014) 294–303.
[42] M. Xu, F. Cao, Y. Zhang, et al., Tanshinone IIA therapeutically reduces LPS-induced acute lung injury by inhibiting inflammation and apoptosis in mice[J], Acta Pharmacol. Sin. 36 (2) (2015) 179–187.
[43] J. Tschopp, K. Schroder, NLRP3 inflammasome activation: the convergence of multiple signaling pathways on ROS production?[J], Nat. Rev. Immunol. 10 (3) (2010) 210–215.
[44] K. Schroder, J. Tschopp, The inflammasomes[J], cell 140 (6) (2010) 821–832.